4-1993

Phase Diagram of a Frustrated Smectic Liquid-Crystal System and the Absence of the Incommensurate Smectic-A_{i_2} Phase

Prem Patel

Li Chen

Satyendra Kumar
Kent State University - Kent Campus, skumar@kent.edu

Recommended Citation

Patel, Prem; Chen, Li; and Kumar, Satyendra (1993). Phase Diagram of a Frustrated Smectic Liquid-Crystal System and the Absence of the Incommensurate Smectic-A_{i_2} Phase. *Physical Review E* 47(4), 2643-2653. doi: 10.1103/PhysRevE.47.2643 Retrieved from https://digitalcommons.kent.edu/phypubs/212

Phase diagram of a frustrated smectic liquid-crystal system and the absence of the incommensurate smectic-A_{i2} phase

Prem Patel, Li Chen, and Satyendra Kumar
Department of Physics and Liquid Crystal Institute, Kent State University, Kent, Ohio 44242-0001
(Received 30 November 1992)

The phase diagram and the structure of smectic-A_d (Sm-A_d) and Sm-A_2 phases of binary mixtures of 4-octyloxy-4′-cyanobiphenyl (8OCB) and 4-*n*-heptyloxyphenyl-4′-cyanobenzoyloxybenzoate (DB7OCN) have been determined by high-resolution x-ray diffraction. This system had previously been reported by Ratna, Shashidhar, and Raja [Phys. Rev. Lett. **55**, 1476 (1985)] to exhibit an incommensurate Sm-A_{i2} phase for concentrations of 8OCB ranging from 25 to 40 mol %. The phase diagram obtained from the present study is in excellent agreement with the mean-field theory of Prost and co-workers [J. Phys. (Paris) **46**, 391 (1985)]. The results of the x-ray study establish that the Sm-A_{i2} phase is, in fact, a coexistence of the Sm-A_d and Sm-A_2 phases at the first-order phase transition between them. Coexistence of the two phases is observed at all concentrations of 8OCB ranging from 35.1 to 0 mol %. At a fixed temperature in the coexistence region, the system evolves towards one phase at a very slow pace. The coexistence region becomes narrower at lower concentrations. Temperature dependence of the smectic wave vectors indicates the presence of a critical point at (physically inaccessible) negative concentrations of 8OCB. The coexistence behavior at the Sm-A_d to Sm-A_2 transition also conforms to the predictions of the theory and resembles the coexistence curve in the proximity of the liquid-gas critical point.

PACS number(s): 61.30.Eb, 64.70.Md, 64.70.Rh, 81.30.Dz

I. INTRODUCTION

Liquid-crystalline compounds with a large electric-dipole moment along the long molecular axis have been known to exhibit a rich smectic-A (Sm-A) polymorphism and multiple reentrance of the nematic and smectic phases. Smectic-A polymorphism in these materials, known as polar liquid crystals, was first observed by Sigaud and co-workers [1,2] and a very elegant mean-field theory was later developed by Prost and co-workers [3–5]. This theory not only successfully explained the formation of known phases but also predicted several phases, the existence of which were later confirmed. At present, there are more than ten smectic phases exhibited [2,6,7] by polar materials including the monolayer Sm-A_1, bilayer Sm-A_2, partially bilayer Sm-A_d, fluid antiphase Sm-$\tilde{A}$, and Sm-A_{cren}. The arrangement of molecules in some of these phases is shown in Fig. 1. Molecules are represented as thin rods with an arrow at one end to denote the longitudinal dipole moment and a lack of inversion symmetry. In the nematic phase, molecules are oriented with their long axis, on the average, parallel to a common direction $\hat{\mathbf{n}}$ known as the director. The direction of molecular dipoles is random and the centers of mass of the molecules lack positional order in this phase. In the smectic phases, the molecules arrange themselves in layers and develop one-dimensional density modulation(s). Within the smectic layers, the molecules are arranged at random. The various smectic-A phases mentioned above differ in layer spacings and dipolar ordering. The Sm-A_1 is a monolayer smectic phase with dipoles oriented randomly up and down within each layer. In this phase, the layer repeat distance is equal to the molecular length l. In the Sm-A_2 phase, dipole moments of the molecules in neighboring layers favor an antiparallel arrangement. The molecular arrangement in the Sm-A_d phase is very similar to the Sm-A_2 phase except that the molecules now have some lengthwise overlap. The effective length of two overlapping molecules in this phase is $2l'$ such that $l<2l'<2l$. The layer spacing $2l'$ in the Sm-A_d phase is strongly temperature dependent. In the Sm-$\tilde{A}$ phase, the local molecular arrangement is the same as in the Sm-A_2 phase but the orientation of the dipoles is modulated in each layer while the antiparallel arrangement subsists along the director giving rise to a two-dimensional rectangular lattice. Just like the Sm-$\tilde{A}$ phase, the crenelated Sm-A_{cren} phase also shows alternation of dipole pairing within a layer, but the neighboring antiphase (antiferroelectric) domains have unequal widths. It has been reported [8] that the width of one domain increases at the expense of the adjacent one with a change in temperature.

Prost and co-workers [5,9,10] have constructed a successful mean-field description of these systems using two complex order parameters ψ_1 and ψ_2,

$$\psi_1(\mathbf{r})=|\psi_1(\mathbf{r})|e^{i\mathbf{q}_1\cdot\mathbf{r}},$$

$$\psi_2(\mathbf{r})=|\psi_2(\mathbf{r})|e^{i\mathbf{q}_2\cdot\mathbf{r}}.$$

The order parameter ψ_1 is associated with antiparallel dipolar pairing while ψ_2 represents the usual smectic mass-density modulation. The two order parameters have natural wave vectors $k_1=2\pi/2l'$ and $k_2=2\pi/l$ which, in general, are different from q_1 and q_2 at which they eventually condense. Wave vectors q_1 and q_2 are determined, in part, by the coupling and the elastic energy terms in the free-energy density:

$$F-F_0=a_1(T-T_{1c})|\psi_1|^2+a_2(T-T_{2c})|\psi_2|^2 D_1|(\Delta+k_1^2)\psi_1|^2+D_2|(\Delta+k_2^2)\psi_2|^2+C_1|\nabla_\perp\psi_1|^2+C_2|\nabla_\perp\psi_2|^2$$
$$+u_1|\psi_1|^4+u_2|\psi_2|^4+2u_{12}|\psi_1|^2|\psi_2|^2-w\ \mathrm{Re}(\psi_1^2\psi_2^*)-v\ \mathrm{Re}(\psi_1\psi_2^*)\ .$$

Here, $a_i(T-T_{ic})$ measures distances from the mean-field transition temperatures T_{1c} and T_{2c} for the fields ψ_1 and ψ_2, respectively, in the absence of any coupling between them. The elastic terms with coefficients D_i describe the spatial modulations and require $q_1^2=k_1^2$ and $q_2^2=k_2^2$. The terms with coefficients C_i depend on gradients of ψ_1 and ψ_2 in a plane perpendicular to $\hat{\mathbf{n}}$ and favor that q_1 and q_2 be parallel to the director. The terms $\psi_1\psi_2^*$ and $\psi_1^2\psi_2^*$ favor lock-in of the two wave vectors at $q_1=q_2$ and $q_1=2q_2$, respectively. Depending on the nature of intermolecular interactions and on the ratio k_2/k_1, one of these two coupling terms generally dominates. The physics of compounds having the ratio $k_2/k_1\sim 2$ is governed by the third-order coupling term with coefficient w, whereas the second-order coupling term with coefficient v is important when k_2/k_1 is close to 1. These competing tendencies are responsible for the formation of a number of polar smectic phases, sometimes referred to as *frustrated* smectics.

Qualitative features of x-ray-diffraction patterns of the polar nematic and smectic-A phases are shown in Fig. 2. In the nematic phase, only orientational order along the director exists and $\psi_1=\psi_2=0$. Diffuse spots at $2q_0=2\pi/l$ and $q'=2\pi/2l'$ $(l<2l'<2l)$, corresponding to molecular length l and weakly associated dimer length $2l'$, respectively, are observed. The presence of two diffuse spots in the nematic phase distinguishes these materials from their nonpolar counterparts which exhibit only one diffuse spot. When only the mass-density wave

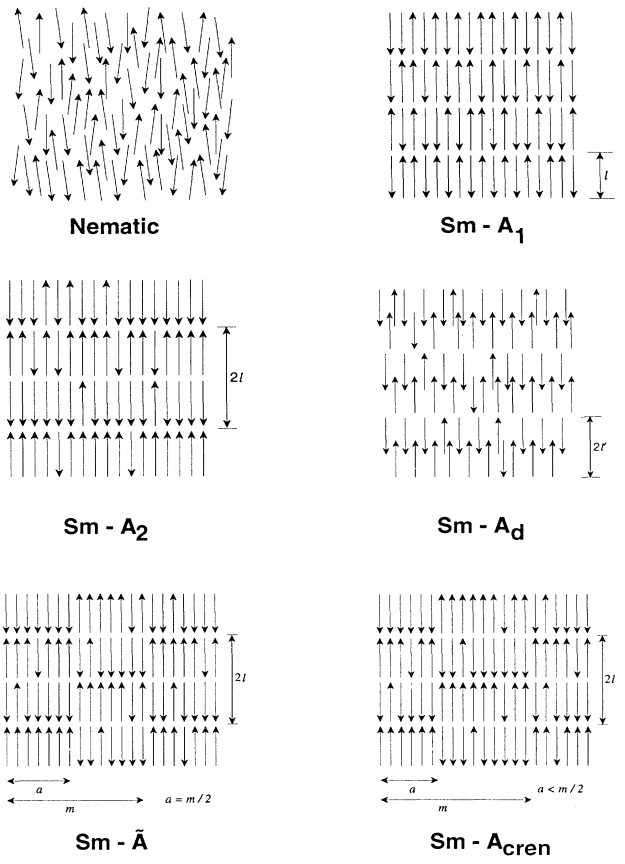

FIG. 1. Schematic representations of the polar nematic and smectic-A phases. The molecules are drawn as thin rods with arrows on one end to denote the longitudinal dipoles. Here, l is the molecular length and $2l'$ $(l<2l'<2l)$ is the effective length of dimerlike molecular arrangements formed in the Sm-A_d phase. The smectic layer spacings of various phases are shown in terms of l and l'. In the Sm-$\tilde{A}$ and Sm-A_{cren} phases, the in-plane modulation has the repeat distance m. In these phases a and $(m-a)$ represent the widths of adjacent antiphase regions as discussed in the text.

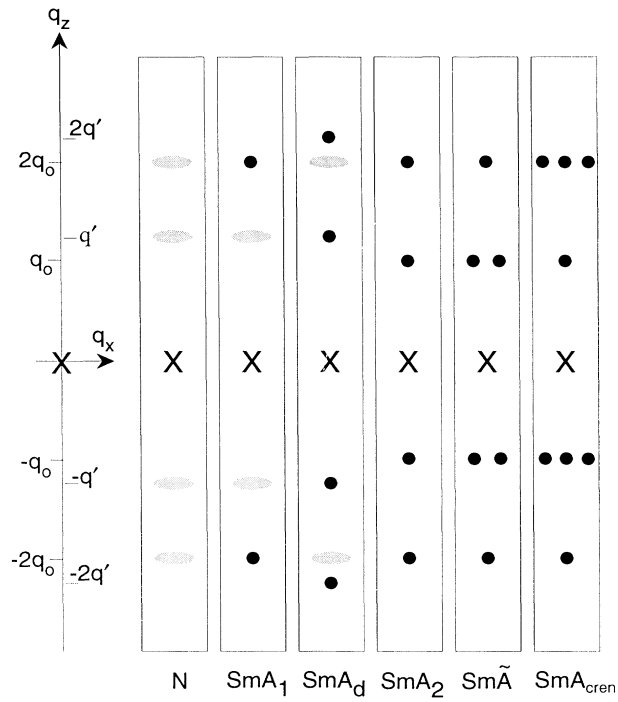

FIG. 2. X-ray-diffraction patterns for the phases exhibited by polar liquid crystals. The solid dots represent quasi-Bragg peaks from smectic structure and the shaded ellipses represent diffuse scattering due to short-range (liquidlike) molecular arrangement. Here, q_z is along the smectic layer normal. The wave number $2q_0=2\pi/l$, l being the molecular length, corresponds to the monolayer (Sm-A_1) phase while $q'=2\pi/2l'$ corresponds to the partial bilayer (Sm-A_d) phase. Note that the Sm-$\tilde{A}$ and Sm-A_{cren} phases have quasi-Bragg reflections with nonzero value of transverse component (q_x) of the scattering vector.

condenses, i.e., $\psi_1=0$ and $\psi_2\neq 0$, then the monolayer Sm-A_1 phase is formed. In this phase molecular dipoles are pointing up and down with equal probability. The x-ray-diffraction pattern of this phase consists of a quasi-Bragg reflection at $2q_0$ and a diffuse peak centered around q'. When both of the order parameters are nonzero, a number of interesting possibilities arise. If wave vectors corresponding to the mass- and polarization-density waves are collinear and $2l'\simeq 2l$, the dominant third-order coupling term with the coefficient w enforces commensurability ($k_2=2k_1$), resulting in the formation of the Sm-A_2 phase. Quasi-Bragg spots are observed at q_0 and $2q_0$ from the Sm-A_2 phase. However, if $\psi_1\neq 0\neq\psi_2$ and $2l'<2l$, as will be the case when molecules are partially overlapping, the Sm-A_d phase with sharp reflections at q', $2q'$, and a diffuse spot at $2q_0$ (corresponding to smectic fluctuations at the monolayer periodicity) is obtained.

The theory also allows the two wave vectors to assume different directions. When the natural wave vector corresponding to ψ_1 is not parallel to $\hat{\mathbf{n}}$, then the Sm-$\tilde{A}$, Sm-A_{cren}, etc., phases are obtained. As a consequence of this escape of $\mathbf{q}_1$ to the second dimension, a modulation of wavelength m develops in the smectic planes. In the Sm-$\tilde{A}$ phase, regions of dipolar pairing of width $a=m/2$ are separated from each other by $m/2$, as shown in Fig. 1. The magnitude of a (and m) depends on the projection of $\mathbf{q}_1$ onto the smectic plane. Regions of antiparallel dipolar pairing form a rectangular lattice in a plane perpendicular to the smectic layers. The diffraction pattern of the Sm-$\tilde{A}$ phase has sharp peaks at $2q_0$ and at two spots, one on either side of the q_0 position, with nonzero q_x components. The situation in the Sm-A_{cren} phase is more complex. In this phase, the regions of antiparallel pairing of width a are separated by similar regions of width $m-a$ ($\neq a/2$) that are displaced by l along $\hat{\mathbf{n}}$. The widths a and m in this phase are temperature dependent. The Sm-A_{cren} phase and its diffraction pattern have been more completely described by Levelut [8].

When the wave vectors corresponding to the two modulations are collinear but their ratio, k_2/k_1, cannot be expressed as a ratio of two integers, then three incommensurate smectic phases are possible [3,10]. The stability of these phases is governed by the incommensurability parameter z defined [9] in terms of the coefficients in the free-energy density and the mismatch between the two natural wave vectors k_1 and k_2 as

$$z=\left[\frac{2D_1u_{12}}{w^2}\right]^{1/2}(k_1^2-\tfrac{1}{4}k_2^2)\ .$$

The incommensurate phases are most likely to form when z and the coefficient C_1 of the gradient term in the free-energy density are large. For small C_1, frustration can be relieved by $\mathbf{q}_1$ escaping to the second dimension, resulting in the fluid antiphase Sm-$\tilde{A}$. When the coupling between order parameters is strong, solitonlike regions of width ξ with two interpenetrating modulations with wave vectors k_2 and k_1 (shown in Fig. 3 by solid and dashed lines) separate Sm-A_2-type lock-in regions of width $(Z-\xi)$. In this *soliton* or Sm-A_{is} phase, the periodicity Z of discommensurations changes with temperature and is expected to diverge at the transition to the Sm-A_2 phase. In x-ray-diffraction experiments, quasi-Bragg reflections at $2q_0$, q'', and $q_s=2q_0-q''$ are expected from this phase and the difference $q''-q_s$ determines Z.

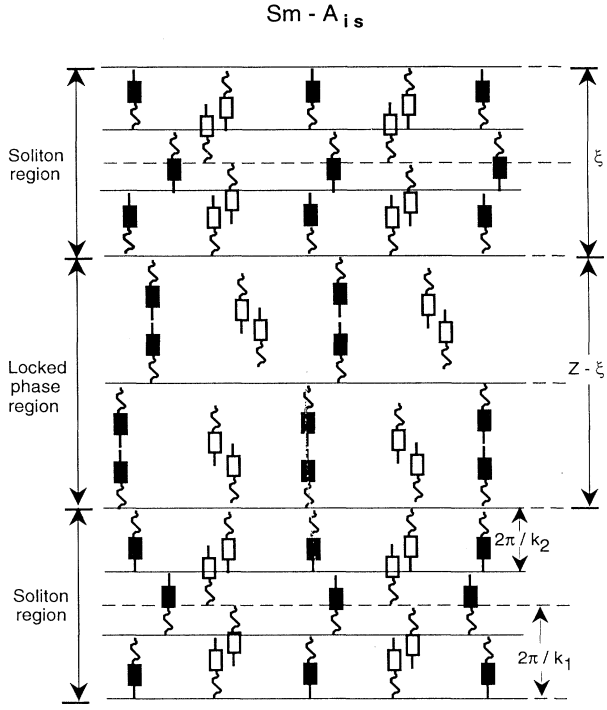

FIG. 3. Real-space representation of the incommensurate soliton Sm-A_{is} phase. The central rigid part of molecules is represented by the rectangle, aliphatic tail by wavy lines, and the dipoles by a short straight line on one side of the rectangle. In this phase, regions of width ξ with two independent wave vectors k_1 and k_2 separate regions of width $Z-\xi$ in which the two modulations are phase locked. The molecules form dimer-like arrangements with no overlap (filled rectangles) or with some lengthwise overlap (unfilled rectangles).

When the coupling between the order parameters is weak, the two periodic modulations can coexist on a microscopic scale. Although not a rigorous representation, the two incommensurate phases, Sm-A_{i1} and Sm-A_{i2}, possible in this weak-coupling limit are shown in Figs. 4 and 5. In the Sm-A_{i1} and Sm-A_{i2} phases, quasi-Bragg reflections are expected at $2q_0$ and q' and at q_0, $2q_0$, and q', respectively. The incommensurate phases [11] are expected to occur much less frequently than the biaxial Sm-$\tilde{A}$ phase as the escape to two dimensions is energetically more favored. Nevertheless they should form under proper conditions.

The existence of the incommensurate smectic-A phases and phase fluctuations has been reported [12,13] in a number of systems. Solitonlike modulations were reported by Brownsey and Leadbetter [14] in the crystalline-E phase of 4-octyl-4'-cyanoterphenyl. Fontes *et al.* [15] also reported strong incommensurate fluctuations in mixtures of DB5 (4-cyano-4-[(4-pentylphenoxy)carbonyl]

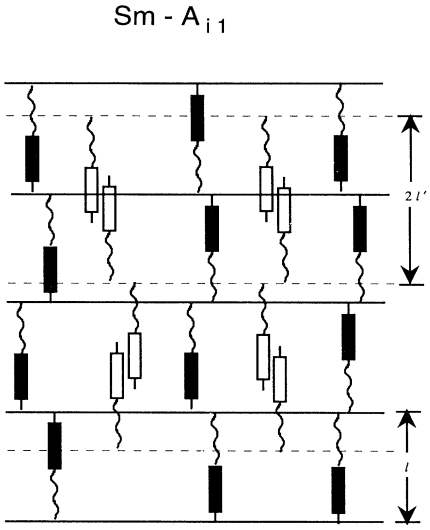

FIG. 4. Real-space representation of the incommensurate Sm-A_{i1} phase. Two interpenetrating smectic modulations with periodicities of l (dark molecules) and $2l'$ (open molecules, with overlapping dimerlike arrangements) coexist in the Sm-A_{i1} phase.

phenyl ester) and T8 (4-octyloxy-4-[2-(4-cyanophenyl)ethenyl] phenyl ester) suggesting close proximity of an incommensurate phase with strongly coupled order parameters. The incommensurate Sm-A_{i2} (initially denoted as Sm-A_{ic}) phase was reported [12] by Ratna, Shashidhar, and Raja in binary mixtures of DB7OCN (4-*n*-heptyloxyphenyl-4′-cyanobenzoloxybenzoate) and 8OCB (4-octyloxy-4′-cyanobiphenyl). They simultaneously observed three x-ray-diffraction peaks, two of which were at incommensurate values of wave vectors and the third peak was a second harmonic of the first one. The values of wave vectors closely corresponded with the wave vectors of the Sm-A_2 and Sm-A_d phases. On the basis of the concentration and temperature dependence of the wave vectors in the Sm-A_{i2} phase, the possibility of it being a simple coexistence of the Sm-A_2 and Sm-A_d phases was ruled out. The absence of x-ray reflections at sums and differences of the observed wave vectors (as expected in the soliton phase) indicated that this was the weakly coupled incommensurate Sm-A_{i2} phase. This discovery stimulated experimental and theoretical interest in this system [16,17]. The subsequent experimental work tended to confirm the existence of this phase. An extension of the mean-field theory [18] succeeded quite remarkably in reproducing the experimental phase diagram of this system.

We have conducted a comprehensive high-resolution x-ray-diffraction study of the smectic phases in eight mixtures of 8OCB and DB7OCN, with 8OCB concentrations ranging from 35.1 to 0.0 mol %. Our results [19] show that the Sm-A_{i2} phase of this system is, in fact, a region of coexistence of the Sm-A_d and Sm-A_2 phases. The phase diagram and the coexistence behavior at the Sm-A_d to Sm-A_2 transition determined from our study are in excellent agreement with the theory.

II. EXPERIMENTAL DETAILS

High-resolution x-ray scattering experiments are carried out using an 18-kW Rigaku RU-300 rotating-anode x-ray generator in conjunction with a two-circle Huber goniometer. A schematic diagram of the experimental setup is shown in Fig. 6. A germanium single crystal, with (111) surface polished, is used as monochromator to select the Cu $K\alpha$ doublet. The diffracted beam is ana-

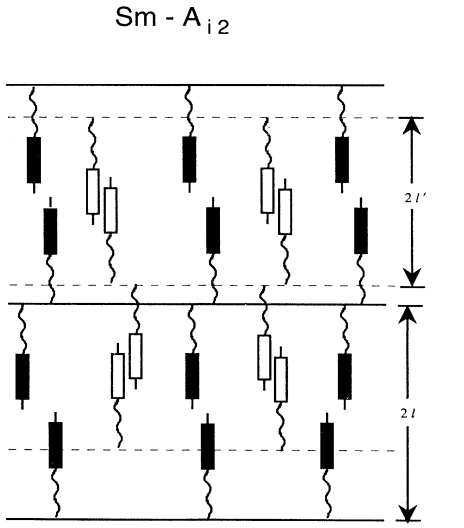

FIG. 5. Real-space representation of the Sm-A_{i2} phase in which Sm-A_d-like (open molecules) and Sm-A_2-like (dark molecules) molecular arrangements coexist throughout the sample.

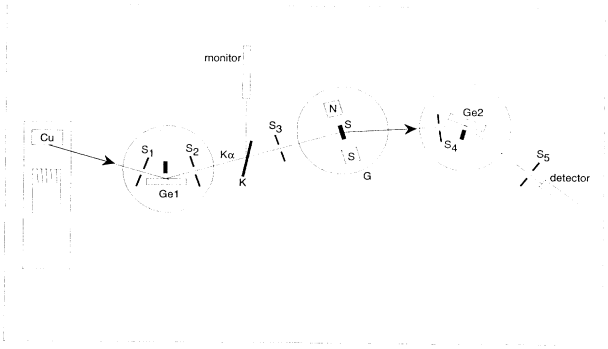

FIG. 6. Schematic representation of the high-resolution x-ray-diffraction experiment. Here, Cu represents the copper target of the Rigaku rotating anode source, and Ge1 and Ge2 are single germanium crystals used as the monochromator to select $K\alpha$ radiation and the analyzer, respectively. G is a two-circle Huber goniometer with angular precision of 0.000 25° for θ and 2θ motions, S_1, S_2, S_3, S_4, and S_5 are collimating slits, S is the sample in the magnetic field produced by a pair of rare-earth permanent magnets N and S, and K represents a thin Kapton sheet used to scatter a small fraction of the beam into the monitor.

lyzed with a second germanium single crystal arranged in a nondispersive geometry. This arrangement affords us a longitudinal resolution $\Delta q_{\parallel}=4\times10^{-4}$ Å^{-1}. The transverse in-plane instrumental resolution is $\Delta q_{\perp}=2\times10^{-5}$ Å^{-1}. The transverse out-of-plane resolution depends on the collimating slits and the sample size. It is measured to be $\Delta q_{\perp}=4\times10^{-2}$ Å^{-1} with a silicon single crystal placed at the center of the diffractometer. The high flux available from the rotating-anode source makes it possible to perform high-resolution experiments even on weakly scattering systems. Evacuated flight paths are used to minimize attenuation and background due to air scattering. The SPEC software package is used to move the spectrometer, perform counting and timing, and to measure and change the sample temperature. The interface is established via a combination of Scientific Solution's LabMaster and IEEE-488 bus boards, and Advanced Control System's MCU-2 stepping motor controllers.

Mixtures of different concentrations, prepared by vigorous stirring and degassing by a repeated freeze-melt process in vacuum, are sealed between two 8-μm-thick Mylar sheets, and a 1.5-mm-thick and 6-mm-inside-diam Teflon O ring. The sample is placed in a two-stage oven with temperature stability and precision of better than ±10 mK. It is aligned by slowly cooling from the nematic phase in a $\sim$2.5-kG magnetic field produced by a pair of rare-earth permanent magnets placed inside the oven. The compound DB7OCN was synthesized using a standard procedure and purified by recrystallization. 8OCB, purchased from BDH Chemicals, was used without further purification.

Primarily, two types of scans, $q_{\parallel}$ scans and ω scans ($\omega=\theta-2\theta_0/2$, where $2\theta_0$ is the position of a selected peak) are performed. During the latter, the detector is fixed at a selected peak position (determined from $q_{\parallel}$ scans) and the intensity of this peak is measured as the sample is rotated about an axis perpendicular to the scattering plane. The $q_{\parallel}$ scans provide information regarding the smectic layer thickness perpendicular to the scattering vector while ω scans, at a particular peak, yield an orientational map of smectic layers of the corresponding thickness. Two reflections from a single phase, for example q_0 and $2q_0$ peaks from the Sm-A_2 phase, must originate from the same scattering volume (domains) in the sample and must have identical ω scans. Conversely, when the ω scans of two peaks are different, they originate from physically different domains in the sample, implying a coexistence of two phases. The ω scans are thus a powerful tool to determine the coexistence.

Longitudinal scans are conducted on magnetically aligned samples to determine the peak positions in various smectic phases. The number of reflections and relationship between their q values help in identifying a phase. The ω scans for each peak obtained in $q_{\parallel}$ scans are used to determine whether they originate from the same scattering volume. In addition to the above two scans, mesh scans are performed in the $q_{\parallel}$-$q_{\perp}$ plane to check for the presence of off-axis peaks which are likely to arise from frustrated smectic phases such as Sm-$\tilde{A}$, Sm-A_{cren}, and Sm-$\tilde{C}$.

III. RESULTS AND DISCUSSION

The temperature dependence of smectic layer spacings corresponding to the q' and q_0 reflections in the Sm-A_d and Sm-A_2 phases of DB7OCN-plus-8OCB mixtures are determined from the $q_{\parallel}$ scans. The results of our measurements at eight different molar concentrations are summarized in Fig. 7.

The 35.1 mol % 8OCB mixture exhibits a Sm-A_d phase above 120 °C and a Sm-A_2 phase below 108 °C. A 12°-wide region between the two phases was previously identified [12] as the incommensurate Sm-A_{i2} phase. The $q_{\parallel}$ and ω scans performed in the three regions are discussed below.

In the Sm-A_d phase, at 121.35 °C, two quasi-Bragg peaks at $q'=0.1328$ Å^{-1} and $2q'=0.2656$ Å^{-1} and a diffuse peak at $2q_0\sim0.2389$ Å^{-1} are observed as shown in Fig. 8(a). At temperatures lower than 120 °C, two additional peaks appear at $q_0=0.1211$ Å^{-1} and $2q_0=0.2422$ Å^{-1}. The peaks at q_0 and $2q_0$ become more intense, while those at q' and $2q'$ grow weaker at lower temperatures and eventually disappear at 108 °C as the system enters the Sm-A_2 phase. At 105.22 °C, the two peaks at $q_0=0.1196$ Å^{-1} and $2q_0=0.2390$ Å^{-1} from the Sm-A_2 phase are shown in Fig. 8(c). The four peaks are present between 120 and 108 °C and their relative intensities change systematically with temperature. At 115.69 °C [Fig. 8(b)], intensities of q_0 and q' peaks become comparable. At this temperature, it is not possible with our high-resolution setup to observe the diffuse peak

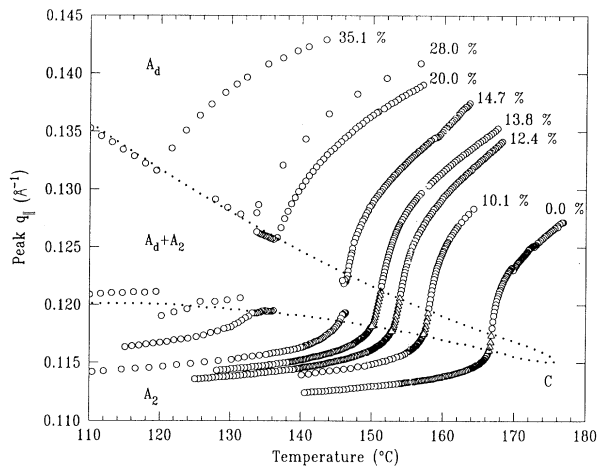

FIG. 7. Temperature dependence of the Sm-A_d and Sm-A_2 wave vectors, q' and q_0, respectively, for eight different concentrations of 8OCB in 8OCB-plus-DB7OCN mixtures. The simultaneous presence of the two peaks over a finite temperature range for concentrations higher than 14 mol % confirms the coexistence of the two phases. At concentrations below 14 mol %, a dramatic increase in peak width and an associated drop in peak intensity are used to infer the coexistence (triangles) as discussed in the text. The dotted line is drawn to approximately represent the outline of the coexistence of the Sm-A_d and Sm-A_2 phases.

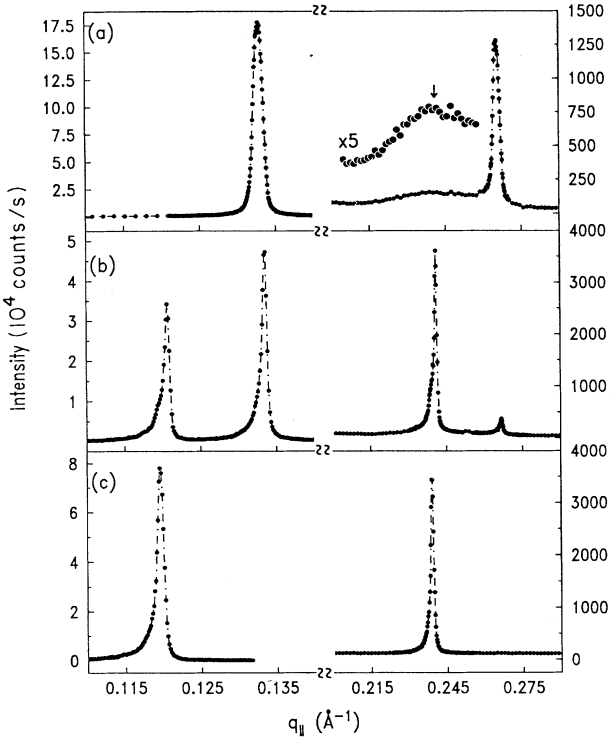

FIG. 8. Longitudinal ($q_\parallel$) scans taken at different temperatures for 35.1-mol% 8OCB in the 8OCB-plus-DB7OCN mixture. (a) In the Sm-A_d phase at 121.35 °C, there are two quasi-Bragg peaks at $q'=0.1328$ Å^{-1} and $2q'=0.2656$ Å^{-1}, and a diffuse peak (also shown on 5× scale) at $2q_0\sim0.2389$ Å^{-1}. (b) In the coexistence region at 115.69 °C, two Sm-A_d peaks at $q'=0.1335$ Å^{-1} and $2q'=0.2667$ Å^{-1}, and two Sm-A_2 peaks at $q_0=0.1206$ Å^{-1} and $2q_0=0.2409$ Å^{-1} are simultaneously present. (c) At 105.22 °C, only two Sm-A_2 peaks at $q_0=0.1196$ Å^{-1} and $2q_0=0.2390$ Å^{-1} remain.

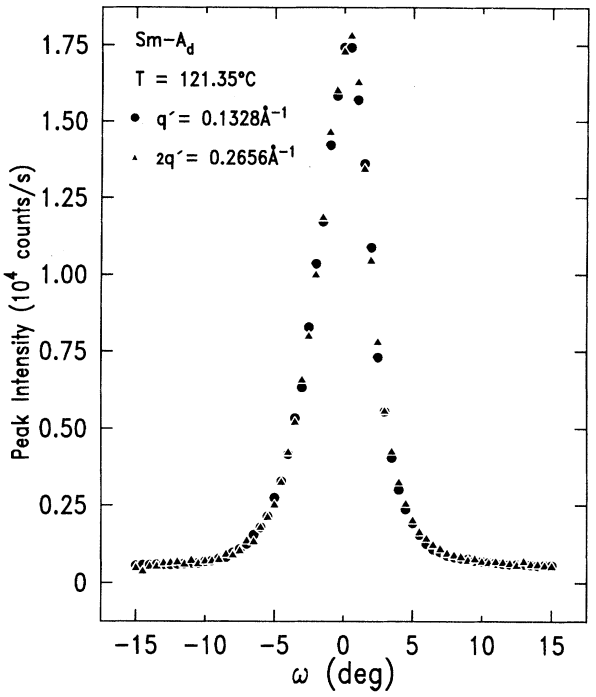

FIG. 9. ω scans through the two Sm-A_d peaks shown in Fig. 8 for the 35.1-mol% 8OCB-plus-DB7OCN mixture possess half-widths of ~2.3°. The $2q'$ peak has been scaled by 2.6 and shifted by 375. The two ω scans, evidently, are identical.

at $2q_0$ in the presence of a sharp peak at the same position. Since the Sm-A_{i2} phase is expected to have three reflections at q_0, q', and $2q_0$, the simultaneous presence of four peaks suggests a coexistence of the Sm-A_d and Sm-A_2 phases.

ω scans taken through the two Sm-A_d peaks at 121.35 °C (Fig. 9) reveal a well-aligned sample with a full width at half maximum (FWHM) of ~2.3°. A mosaic scan of the $2q'$ peak has been scaled by 2.6 and shifted by 375 along the intensity axis. The two ω scans are identical, confirming that both reflections originate from the same scattering volume and that the corresponding mass-density modulations are collinear. The sample mosaic is found to gradually broaden at lower temperatures as the weak external field of 2.5 kG becomes ineffective in maintaining the molecular alignment in the smectic phases.

The shapes of ω scans taken through the two Sm-A_d peaks at 119.35 °C are similar as expected [Fig. 10(a)]. ω scans of the two Sm-A_2 reflections at 119.35 °C [Fig. 10(b)] are also identical but quite different from the Sm-A_d peaks. The FWHM of the ω scans of the two Sm-A_d reflections is ~4.7°, while that of the two Sm-A_2 peaks is ~7.2°. The ω scans for all quasi-Bragg reflections from a Sm-A_{i2} phase should have been identical. Differences in the ω scans show that reflections from the Sm-A_d and Sm-A_2 phases originate from different parts of the sample confirming their coexistence. Small differences between the two curves in Fig. 10(b) can be attributed to the fact that the scans are taken at different times while the sample mosaic is changing. ω scans taken at a fixed temperature in this coexistence region evolves very slowly with time. To qualitatively understand this evolution, peak intensities of ω scans through Sm-A_d and Sm-A_2 reflections at 116.30 °C have been plotted against time in Fig. 11. The solid lines represent exponential dependences with a single time constant of approximately 12.4 h for both peaks. Growth of the Sm-A_2 peak and disappearance of the Sm-A_d peak at the same rate shows that the sample is gradually changing to the Sm-A_2 phase, providing further proof of their coexistence. ω scans through the two Sm-A_2 peaks at 108 °C are found to be identical, as all parts of the sample are now in the same phase.

The possibility of the $2q'$ peak being due to multiple scattering can be ruled out on account of the following three arguments. First, a multiple-scattering peak must have a different mosaic than the primary reflection. The $2q'$ peak here has the same mosaic as the q' peak. Second, the ratio of intensities of the two peaks increases

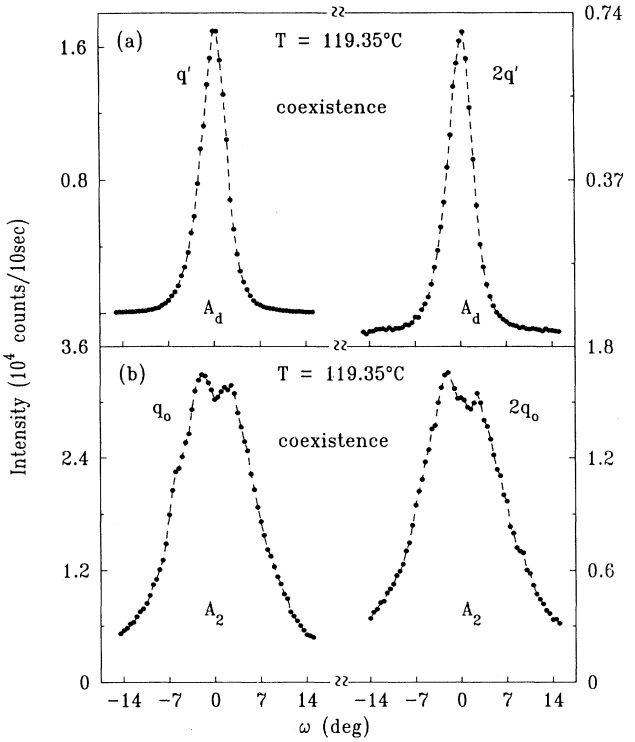

FIG. 10. ω scans for the 35.1-mol % 8OCB-plus-DB7OCN mixture through (a) the two Sm-A_d peaks at $q'=0.1313$ Å^{-1} and $2q'=0.2626$ Å^{-1} and (b) the two Sm-A_2 peaks at $q_0=0.1211$ Å^{-1} and $2q_0=0.2422$ Å^{-1} in the coexistence region, at 119.35 °C.

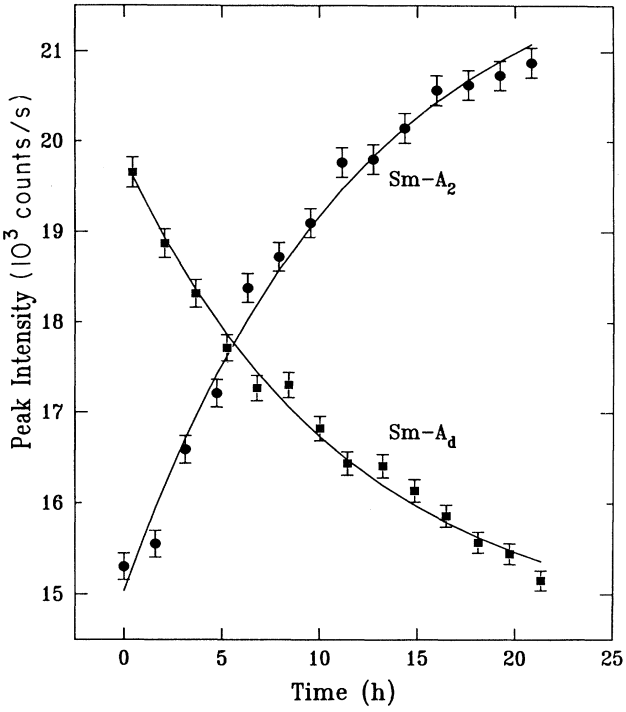

FIG. 11. Time dependence of the peak intensities at $q_0=0.1206$ Å^{-1} of the Sm-A_2 phase and $q'=0.1336$ Å^{-1} of the Sm-A_d phase (different vertical scales) at a fixed temperature (116.30 °C) in the coexistence region after the sample is cooled from the Sm-A_d phase. The solid lines represent exponential fits both with the time constant of approximately 12.4 h.

with decreasing temperature while the mosaic becomes gradually broader, which is contrary to the expectation from the multiple-scattering peak. Furthermore, this ratio is a smooth function of temperature as shown in Fig. 12. There is no conceivable way to expect this behavior from a peak due to multiple scattering when the sample mosaic is changing. Again, if present, it would behave quite the opposite. In fact, the temperature dependence of this ratio is a measure of how the order parameter ψ_1 develops as the Sm-A_2 phase is approached. It is and should be independent of the sample mosaic. Lastly, the intensity of the $2q'$ peak is too high to be a multiple-scattering peak. We measure, at 115.69 °C, the intensity of the q' peak $I(q')$, to be $\sim 19\,000$ s^{-1} for an incident beam intensity of $\sim 6\,000\,000$ s^{-1}. The ratio of the diffracted to incident beam intensity for the q' peak is $\sim 3\times 10^{-3}$. Thus, for the $2q'$ peak to be due to multiple scattering, its intensity must be $<(3\times 10^{-3})I(q')$. But in practice, $I(2q')\sim(1\times 10^{-2})I(q')$.

Deuterium NMR spectra recently obtained by Ukleja, Neubert, and Keast [20] for 35.0-mol % 8OCB-d2 (deuterated in the α position) show the existence of two types of order on cooling into the so-called "incommensurate" region, providing an independent proof of this coexistence.

The 28.0-mol % mixture exhibits a Sm-A_d phase above 133 °C and a Sm-A_2 phase below 127 °C. The 6 °-wide re-

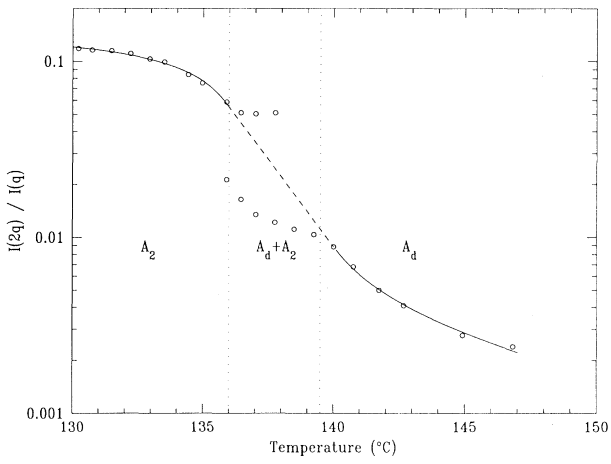

FIG. 12. The ratio of intensities of the second to first reflection in the Sm-A_d and Sm-A_2 phases of 280-mol % 80CB mixture. This ratio increases with decreasing temperature and qualitatively represents the relative growth of the order parameter ψ_2 at the Sm-A_d to Sm-A_2 transition. Wide coexistence at this phase transition is evident. Lines through the data points are drawn as a guide to the eye.

gion between the two phases is also found to be a coexistence region of the Sm-A_d and the Sm-A_2 phases. In this region at 131.5 °C, mesh scans are performed in the $q_{\parallel}$-$q_{\perp}$ plane in the proximity of the $q'=0.1334$ Å^{-1} peak of the Sm-A_d phase, as shown in Fig. 13. No other peaks are found in its vicinity, thus ruling out the possibility of it being the Sm-$\tilde{A}$, Sm-A_{cren}, or Sm-$\tilde{C}$ phase.

In order to optically observe the texture in this region, a microscope slide is prepared with lecithin-treated glass plates. Homeotropic alignment is obtained in the Sm-A_d phase of the 28.0-mol % mixture. Upon cooling into the intermediate region, domains of very slightly different contrast separated by bright and relatively sharp boundaries which appeared to form loops are observed as shown in Fig. 14. This, evidently, is due to phase separation accompanying the coexistence of the Sm-A_2 and Sm-A_d phases. Similar lines were also present in the textures reported in Ref. [17]. These sharp grain boundaries become broad with time as the molecules diffuse across them. The texture becomes homeotropic again without any clearly visible boundaries as the sample is cooled to the Sm-A_2 phase.

Similar coexistence of the Sm-A_d and Sm-A_2 phases is also observed at much lower concentrations of 8OCB than the lowest (25 mol %) reported previously for the Sm-A_{i2} phase. The width of the coexistence region decreases with decreasing concentration. As shown in Fig. 7, the 20.0- and 14.7-mol % mixtures have coexistence re-

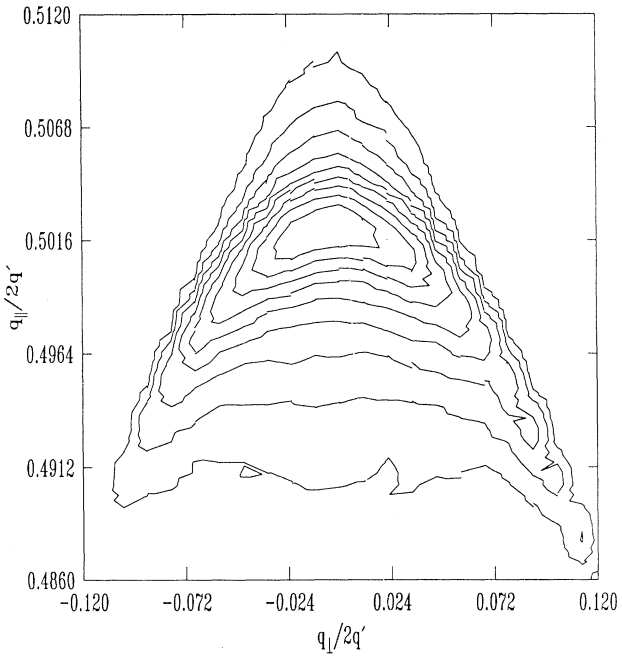

FIG. 13. Equal-intensity contour plots in the $q_{\parallel}$-$q_{\perp}$ plane in the vicinity of q' reflection in the coexistence region. Contours are drawn at 90, 80, 70, 60, 50, 40, 30, 20, and 10% of peak intensity. These measurements were made at 131.50 °C for the 28.0-mol % 8OCB-plus-DB7OCN mixture. The absence of off-axis peaks rules out the possibility of this region being the Sm-$\tilde{A}$, the Sm-A_{cren}, or the Sm-$\tilde{C}$ phase.

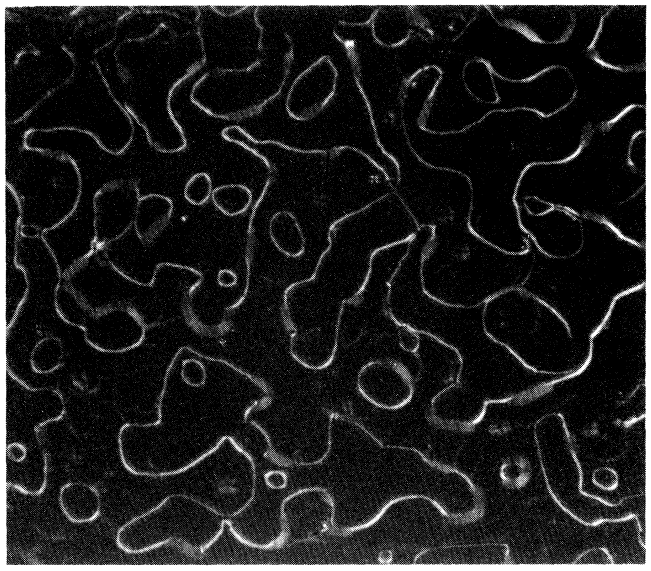

FIG. 14. Upon cooling the homeotropically aligned Sm-A_d phase of the 28.0-mol % mixture into the intermediate region, domains of slightly different contrast separated by bright and relatively sharp lines forming loops are observed. These loops become diffuse with time and disappear upon cooling into the Sm-A_2 phase.

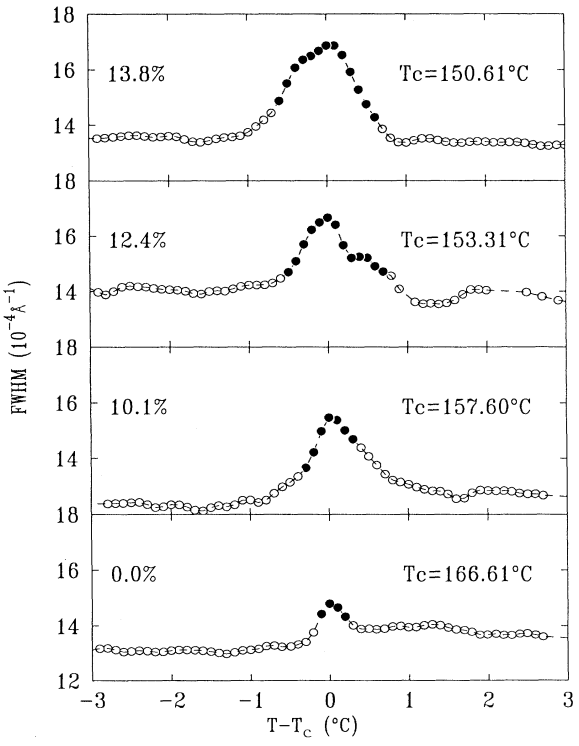

FIG. 15. Temperature dependence of full peak width at half maximum of the q' peak, which evolves into the q_0 peak, for 13.8, 12.4, 10.1, and 0.0-mol % 8OCB in the 8OCB-plus-DB7OCN mixtures. An increase in the peak width near the Sm-A_d to Sm-A_2 transition is due to simultaneous presence of unresolved q' and q_0 peaks from the Sm-A_d and Sm-A_2 phases, respectively.

gions of 2.5 and 0.7 °C, respectively. The q' and q_0 peaks cannot be resolved for concentrations lower than 14 mol %. However, the $q_{\|}$ peaks, at concentrations lower than 14 mol %, show an increase in their width (Fig. 15) accompanied by a decrease in peak intensity (Fig. 16) at the transition (inflection point on the q vs T curve in Fig. 7) from the Sm-A_d to the Sm-A_2 phase. We believe this is to be due to the presence of reflections from both phases. The q_0 and q' peaks constitute the composite peak of increased width as they are now unresolved. We estimate the width of coexistence range by monitoring the width and peak intensity. The points that fall in this region are shown as filled circles in Figs. 15 and 16. Evidently, the Sm-A_d and Sm-A_2 phases coexist even in pure DB7OCN, suggesting that the critical point lies at negative concentrations of 8OCB. It should be pointed out that the observed coexistence in these mixtures (and even pure DB7OCN) is due to the fact that the system equilibrates sluggishly and one makes inequilibrium measurements over the experimental time scales.

Phase separation at a first-order transition should result in the formation of domains corresponding to the high- (disordered) and the low- (ordered) temperature phases. The concentrations of these domains are expected to change with temperature and follow the phase-boundary lines defining the coexistence region, in conformity with the lever rule. The data for the Sm-A_d segment of q vs T curves for different concentrations in the coexistence region should fall on a single curve representing the phase boundary. Similar arguments hold for the Sm-A_2 segment. The results shown in Fig. 7 do not completely fulfill this expectation because the system does not fully reach equilibrium during our experiments. But our results are closer to this expectation than those previously published [12]. The equilibrium time constants appear to be very long and one may have to wait for several days at every temperature in order to measure equilibrium behavior.

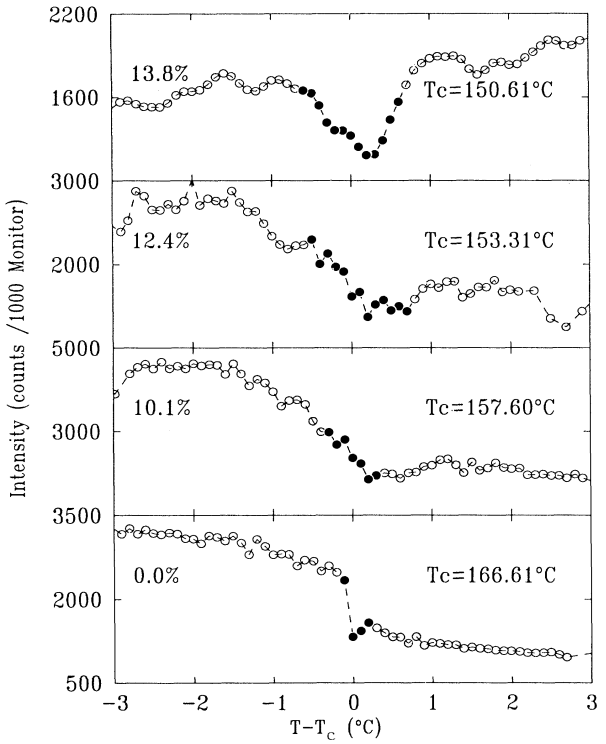

FIG. 16. Temperature dependence of peak intensity of q' reflection, which evolves into the q_0 peak, for 13.8, 12.4, 10.1, and 0.0-mol % 8OCB in the 8OCB-plus-DB7OCN mixtures. The decrease in peak intensity and the associated increase in peak width (Fig. 15) near the Sm-A_d to Sm-A_2 transition are due to the simultaneous presence of the q_0 and q' reflections from the two phases.

The x-ray scans discussed above are performed while cooling the sample from a well-aligned Sm-A_d phase. Heating scans are not possible due to poor initial alignment of sample in the low-temperature Sm-A_2 phase. Heating from intermediate temperatures results in loss of alignment due to strong temperature dependence of q' and layer undulations that develop upon heating. A second scan on the same sample results in entirely different q vs T curves, suggesting a very different concentration. In subsequent scans, the apparent concentration of the sample is found to unpredictably change from scan to scan. Decomposition of the sample does not appear to be responsible for this behavior as it would have given rise to a systematic change in sample concentration (purity). The results are reproducible when the scans are repeated on a virgin sample. We believe that the observed concentration changes in subsequent scans is due to phase separation accompanied by concentration changes at the first-order Sm-A_d to Sm-A_2 transition. Further credence to this belief comes from the fact that the peaks (Fig. 8) obtained from $q_{\|}$ scans in the coexistence and Sm-A_2 regions are strongly asymmetric, indicating a distribution of layer spacing d across the sample due to a change in local concentration.

The Sm-A_2 and Sm-A_d phases belong to the same symmetry class [4], differing from each other only in the value of the wave vectors and the magnitude of Ψ_2. There should be either a first-order transition between the two phases or a continuous evolution from one phase to the other. The line of first-order Sm-A_d to Sm-A_2 phase transitions should terminate at a critical point as predicted theoretically by Barois, Prost, and Lubensky [4]. This has been experimentally confirmed for a number of systems exhibiting the Sm-A_d to Sm-A_2 phase transitions, for example, mixtures of 9OBCB (4-*n*-nonyloxybiphenyl-4′-cyanobenzoate) and 11OPCBOB (4-*n*-undecyloxyphenyl-4′-[4″-cyanobenzyloxy] benzoate) [21] and the tenth and eleventh homologs of *n*OPCBOB (4-*n*-alkyloxyphenyl-4′-[4″-cyanobenzyloxy] benzoate) series [22]. In these systems, a continuous supercritical transformation of the Sm-A_d into the Sm-A_2 phase is observed beyond the critical point. Temperature dependence of wave vectors (Fig. 7) in the vicinity of the critical point C is in good agreement with the calculated dependence [4]. Theoretical considerations suggest [4] that the Sm-A_d to Sm-A_2 transition is analogous to the liquid-gas transition terminating at a critical point which belongs to the 3d Ising universality class. However, more

recent renormalization-group calculations suggest a new universality class with an upper critical dimension of 6 [23,24].

High-precision heat-capacity studies of this system, conducted by Das *et al.* [16], had shown that the heat-capacity peak height at the Sm-A_d to Sm-A_2 transition grew weaker and broader as the concentration of 8OCB was increased. Rounded C_p peaks were observed at this transition even in pure DB7OCN. These results suggested that the critical point on this phase boundary should be close to pure DB7OCN in accordance with our conclusions. However, with increasing 8OCB concentration the system was believed to move away from the critical point into a supercritical region which explained the broadening of the heat-capacity peaks. Our results, on the other hand, show that this broadening arises due to increasing coexistence. An increase in the 8OCB concentration moves the system away from the critical point but along the first-order transition line. Thus, the heat-capacity results are, from a different perspective, consistent with our results and conclusions. The ΔC_p peaks at 8OCB concentrations higher than 24 mol % became slightly broader and asymmetric and exhibited two "kinks." The positions of the kinks were considered to be the Sm-A_d–Sm-A_{ic} and Sm-A_{ic}–Sm-A_2 transition temperatures. We interpret these "kinks" as marking the beginning and the end of the coexistence.

The phase diagram taken from Ref. [12] has been replotted (Fig. 17), in light of our results, with DB7OCN concentration along the abscissa. The dotted lines represent the measured coexistence at the first-order Sm-A_d–Sm-A_2 (dashed line) transition. This diagram now resembles the upper part of a theoretical phase diagram [Fig. 3(b) in Ref. [4]] without any incommensurate phases.

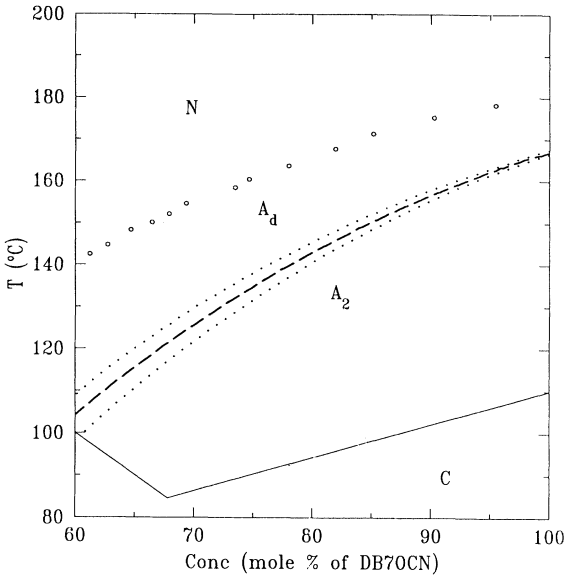

FIG. 17. The phase diagram of the 8OCB-plus-DB7OCN system replotted with the DB7OCN concentration along the abscissa. The dotted curves approximately define the boundaries of the Sm-A_d to Sm-A_2 coexistence and the dashed line in this region represents the first-order Sm-A_d to Sm-A_2 transition.

IV. SUMMARY

We find that the Sm-A_d and Sm-A_2 coexistence region extends to pure DB7OCN and becomes wider as the concentration of 8OCB is increased. No incommensurate smectic-A phases are found in this system. However, our results do not preclude the existence of incommensurate phases in more suitable materials. The phase diagram of the 8OCB-plus-DB7OCN system as redrawn in Fig. 17 is in good agreement with a theoretical phase diagram. The coexistence at the first-order Sm-A_d to Sm-A_2 transition, represented by a dashed line, resembles the theoretically obtained diagram and mimics the behavior at the liquid-vapor critical point.

ACKNOWLEDGMENTS

We thank T. C. Lubensky, C. W. Garland, J. Prost, P. A. Heiney, A. Saupe, D. L. Johnson, and R. Shashidhar for very helpful discussions. The authors are grateful to M. E. Neubert and Sandy Keast for synthesizing high-quality samples. This research was supported by the National Science Foundation under Grant No. DMR-88-19680 and in part by Science and Technology Center Grant No. DMR-89-20147.

[1] G. Sigaud, F. Hardouin, and M. F. Achard, Phys. Lett. **72A**, 24 (1979).
[2] G. Sigaud, M. F. Achard, F. Hardouin, and H. Gasparoux, J. Phys. (Paris) Colloq. **40**, C3-356 (1979).
[3] J. Prost, J. Phys. (Paris) **40**, 581 (1979).
[4] P. Barois, J. Prost, and T. C. Lubensky, J. Phys. (Paris) **46**, 391 (1985).
[5] J. Prost and P. Barois, J. Chim. Phys. **80**, 83 (1983).
[6] F. Hardouin, A. M. Levelut, and G. Sigaud, J. Phys. (Paris) **42**, 71 (1981).
[7] G. Sigaud, F. Hardouin, M. F. Achard, and A. M. Levelut, J. Phys. (Paris) **42**, 107 (1981).
[8] A. M. Levelut, J. Phys. (Paris) Lett. **45**, L603 (1984).
[9] P. Barois, J. Pommier, and J. Prost, in *Solitons in Liquid Crystals,* edited by L. Lam and J. Prost (Springer-Verlag, Berlin, 1992), Chap. 6.
[10] J. Wang and T. C. Lubensky, J. Phys. (Paris) **45**, 1653 (1984).
[11] J. Prost, in *Proceedings of the Conference on Liquid Crystals of One- and Two-Dimensional Order and Their Applications,* edited by W. Helfrich and G. Heppke (Springer-Verlag, Berlin, 1980), p. 125.
[12] B. R. Ratna, R. Shashidhar, and V. N. Raja, Phys. Rev. Lett. **55**, 1476 (1985).

[13] R. Shashidhar and B. R. Ratna, Liq. Cryst. **5**, 421 (1989).
[14] G. J. Brownsey and A. J. Leadbetter, Phys. Rev. Lett. **44**, 1608 (1980).
[15] E. Fontes, P. Heiney, P. Barois, and A. M. Levelut, Phys. Rev. Lett. **60**, 1138 (1988).
[16] P. Das, K. Ema, C. W. Garland, and R. Shashidhar, Liq. Cryst. **4**, 581 (1989).
[17] B. R. Ratna, R. Shashidhar, and V. N. Raja, in *Incommensurate Crystals, Liquid Crystals, and Quasi-Crystals,* edited by J. F. Scott and N. A. Clark (Plenum, New York, 1987), p. 259.
[18] P. Barois, Phys. Rev. A **33**, 3632 (1986).
[19] S. Kumar, L. Chen, and V. Surendranath, Phys. Rev. Lett. **67**, 322 (1991).
[20] P. Ukleja, M. E. Neubert, and S. Keast, The 14th International Liquid Crystal Conference, Book of Abstracts (1992), Vol. 1, p. 440.
[21] R. Shashidhar, B. R. Ratna, S. Krishna Prasad, S. Somasekhara, and G. Heppke, Phys. Rev. Lett. **59**, 1209 (1987).
[22] S. Quentel, G. Heppke, S. Krishna Prasad, S. Pfeiffer, and R. Shashidhar, Mol. Cryst. Liq. Cryst. Lett. **7**, 85 (1990).
[23] Y. Park, T. C. Lubensky, P. Barois, and J. Prost, Phys. Rev. A **37**, 2197 (1988).
[24] Y. Park, T. C. Lubensky, and J. Prost, Liq. Cryst. **4**, 435 (1989).

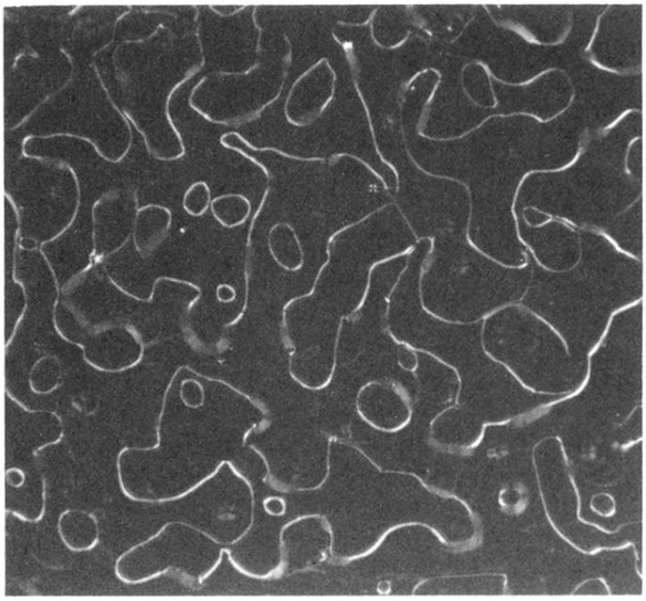

FIG. 14. Upon cooling the homeotropically aligned Sm-A_d phase of the 28.0-mol % mixture into the intermediate region, domains of slightly different contrast separated by bright and relatively sharp lines forming loops are observed. These loops become diffuse with time and disappear upon cooling into the Sm-A_2 phase.